

Spectroscopy of doubly-charmed baryons from lattice QCD

M. Padmanath,^{1,*} Robert G. Edwards,^{2,†} Nilmani Mathur,^{3,‡} and Michael Peardon^{4,§}
(For the Hadron Spectrum Collaboration)

¹*Institute of Physics, University of Graz, 8010 Graz, Austria.*

²*Jefferson Laboratory, 12000 Jefferson Avenue, Newport News, VA 23606, USA*

³*Department of Theoretical Physics, Tata Institute of Fundamental Research,
Homi Bhabha Road, Mumbai 400005, India.*

⁴*School of Mathematics, Trinity College, Dublin 2, Ireland*

We present the ground and excited state spectra of doubly charmed baryons from lattice QCD with dynamical quark fields. Calculations are performed on anisotropic lattices of size $16^3 \times 128$, with inverse spacing in temporal direction $a_t^{-1} = 5.67(4)$ GeV and with a pion mass of about 390 MeV. A large set of baryonic operators that respect the symmetries of the lattice yet which retain a memory of their continuum analogues are used. These operators transform as irreducible representations of $SU(3)_F$ symmetry for flavor, $SU(4)$ symmetry for Dirac spins of quarks and $O(3)$ for spatial symmetry. The distillation method is utilized to generate baryon correlation functions which are analysed using the variational fitting method to extract excited states. The lattice spectra obtained have baryonic states with well-defined total spins up to $\frac{7}{2}$ and the pattern of low lying states does not support the diquark picture for doubly charmed baryons. On the contrary the calculated spectra are remarkably similar to the expectations from models with an $SU(6) \times O(3)$ symmetry. Various spin dependent energy splittings between the extracted states are also evaluated.

PACS numbers: 12.38.Gc, 14.20.Mr

I. INTRODUCTION

The study of hadrons containing charm quarks has recently undergone a renaissance. This resurgence of interest started with the discovery of new resonances in the charmonium system as well as a few charmed baryons. So far, emphasis has been given to the study of the meson sectors both theoretically and experimentally, while heavy baryon physics has received substantially less attention. Similar to charm mesons, a comprehensive study of charm baryons can provide similar insight into the strong interaction. However, in comparison to the many light and strange baryon states, only a handful of charm baryons have been discovered and a reliable determination of the quantum numbers of most of these observed charmed baryons has yet to be made [1]. Only very recently a few excited singly charmed baryons were discovered. Similarly, there is no observation for triply-charmed baryons although QCD clearly predicts such states. For doubly-charmed baryons, only SELEX reported the discovery of five resonances and interpreted those as $\Xi_{ccd}^+(3443)$, $\Xi_{ccd}^+(3520)$, $\Xi_{ccu}^{++}(3460)$, $\Xi_{ccu}^{++}(3541)$ and $\Xi_{ccu}^{++}(3780)$ [2, 3]. Later they confirmed the $\Xi_{ccd}^+(3520)$ state in two different decay modes ($\Xi_{cc}^+ \rightarrow \Lambda_c K^- \pi^+$; $\Xi_{cc}^+ \rightarrow p D^+ K^-$) at a mass of 3518.7 ± 1.7 MeV with an average lifetime less than 33 *fs* [4]. However, these states have *not* been observed either by BABAR [5], Belle [6, 7] in e^+e^- annihilation experiments or by LHCb at baryon-baryon collider experiments at CERN [8]. In SELEX, production of doubly charm baryons with a large cross section occurred through baryon-baryon interactions which is totally inconsistent with fragmentation production. Further, the helicity angular distribution analysis also suggests that the pair of states, $\{\Xi_{cc}^+(3443), \Xi_{cc}^{++}(3460)\}$ and $\{\Xi_{cc}^+(3520), \Xi_{cc}^{++}(3541)\}$ form isospin doublets with isospin splittings 17 and 21 MeV respectively. There is no precise understanding of these unusually large isospin splittings observed in the doubly charm baryons, unlike the small isospin splittings in the case of light and singly charmed baryons. An explanation may be possible if the coulombic electro-magnetic effect is much larger than strong interaction effect, leading to these baryons having a very compact size [9]. In summary, the experimental status of doubly-charmed baryons has not been settled, however it is expected that consolidated analysis of large data collected from the ongoing experiments at LHCb and future experiments like PANDA @FAIR, and Super Belle will shed further light.

Doubly-charmed baryons are interesting systems as they provide a unique insight into the nature of the strong force

*Electronic address: padmanath@theory.tifr.res.in

†Electronic address: edwards@jlab.org

‡Electronic address: nilmani@theory.tifr.res.in

§Electronic address: mjp@maths.tcd.ie

in the combined presence of both slowly moving heavy quarks along with the relativistic motion of a light quark. The excited spectra of these states and the splittings between them can help to understand how the collective degrees of freedom give rise to excitations in these systems. A comparison of these excitations with the corresponding spectra of singly and triply-charmed baryons, where the number of charm quark is one less and one more respectively, will be helpful to get information about quark-quark interactions. Doubly-charmed baryons are characterized by two widely separated scales: the low momentum scale, of order Λ_{QCD} , of the light quark and the relatively heavy charm quark mass. A doubly-heavy baryon can be treated as a bound state of a heavy antiquark and a light quark in the limit when the typical momentum transfer between the two heavy quarks is larger than Λ_{QCD} [10, 11]. In this limit of quark-diquark symmetry, $QQq \leftrightarrow \bar{Q}q$, one can get definite prediction of spin dependent energy splittings [12, 13]. It was argued [14, 15] that because of heavy-quark symmetry, the doubly heavy baryons can be viewed as ultraheavy mesons, $[QQ]q \sim Q'q$ and the hyperfine mass splittings in these systems are suppressed. Moreover, the doubly heavy baryon ground state of the form $[QQ]_{J=1}q$ will consist of chiral multiplets containing spin $(1/2^+, 3/2^+)$ heavy spin fields [14]. It is thus interesting to study these spin splittings to determine if the charm quark is sufficiently heavy to respect this quark-diquark symmetry. Doubly-charmed baryons have been studied over the years using various theoretical methods such as the non-relativistic [16–18] as well as relativistic [19, 20] quark models, heavy-quark effective theory [21], QCD sum rules [22–26], Feynman-Hellmann theorem [27], mass formula [28] and Skyrminion model [29].

In light of existing and future experimental efforts to observe doubly-charmed baryons, it is desirable to have first principle predictions from lattice QCD. A quantitative description of the spectra of doubly-charmed baryons from the non-perturbative method of lattice QCD is valuable as it will enable a comparison between the lattice-computed spectra of doubly-charmed baryons to those obtained from potential models which have been successful for charmonia. Moreover, all results from such a first principles calculation will be predictions and thus naturally can provide crucial inputs to current and future experimental discovery. Given this significance of doubly-charmed baryons, it is desirable to study these states comprehensively using lattice QCD. Lattice QCD groups have studied the ground states of the doubly-charmed baryons using quenched NRQCD [30], quenched QCD with relativistic quarks [31–33], and full QCD [34–41] calculations. However, all previous lattice calculations involve only the spin 1/2 and spin 3/2 ground state spectrum of Ξ_{cc} and Ω_{cc} . It is expected that much more information about the interactions between two charm quarks and between charm and light quarks can be obtained by computing the excited state spectra of these baryons, including in particular the spin-dependent energy splittings, as well as by studying similar spectra for other spin-parity channels. Towards this goal, we report here the first attempt to compute the excited state spectra of doubly-charmed baryons using dynamical lattice QCD. The ground states for each spin-parity channel as well as their excited states up to spin 7/2 are computed and a few spin-dependent energy splittings are also studied. Similar studies of triply-charmed baryons have already been reported in Ref. [42], and in a subsequent publication we will report results on singly charmed baryons.

To extract the excited states of doubly-charmed baryons we follow the same procedure used in previous calculations for mesons [43–48] and baryons [42, 49–51]. The gauge configurations we use are generated with 2+1 flavour clover fermions on anisotropic lattices [52, 53]. For the charm quarks we also use clover fermions which are $\mathcal{O}(a)$ improved at tree level in tadpole-improved perturbation theory. A large set of baryon operators which are first constructed in the continuum and then subduced into various lattice irreps [49] are used for this calculation. These operators transform as irreducible representations of $SU(3)_F$ symmetry for flavor, $SU(4)$ symmetry for Dirac spins of quarks and $O(3)$ symmetry for orbital angular momenta. Baryon correlation functions are generated by using the “distillation method” [54] and then variational fitting method is utilized to extract excited energies as well as to reliably determine the spins of these states.

The layout of the paper is as follows. In the next section, we briefly describe lattice details, operator construction, the construction and analysis of correlation functions and our procedure for identifying the continuum spins of extracted states, which are already detailed earlier in Refs. [42–51, 54]. In section III we present our results giving details of energy splittings in subsection IIIA. Finally, a summary of the work is presented in section IV.

II. COMPUTATIONAL METHODS

Over the last several years the Hadron Spectrum Collaboration (HSC) has adopted a dynamical anisotropic lattice formulation to extract highly excited hadron spectra. In this approach one uses a much finer temporal lattice spacing than in the spatial directions and exploits this higher resolution to extract highly excited states which decay rapidly at large Euclidean time separations with increasing noise to signal ratio. On the other hand, this avoids the computational cost that would come if one reduces the spacing in all directions.

A. The lattice action

We used the tree-level Symanzik-improved gauge action and the anisotropic Shekholeslami-Wohlert fermion action with tree-level tadpole improvement and three-dimensional stout-link smearing of gauge fields for this work. The details of the formulation of actions as well as the method used to tune the anisotropic parameters can be found in Refs. [52, 53]. In Table I we show the lattice action parameters of the gauge-field ensembles used in this work. We

Lattice size	$a_t m_\ell$	$a_t m_s$	N_{cfgs}	m_π/MeV	m_K/m_π	$a_t m_\Omega$
$16^3 \times 128$	-0.0840	-0.0743	96	391	1.39	0.2951(22)

TABLE I: Details of the gauge-field ensembles used. N_{cfgs} is the number of gauge-field configurations.

used the Ω -baryon mass to determine the lattice spacing and obtained $a_t^{-1} = 5.67(4)$ GeV. With an anisotropy of close to 3.5, this leads to $a_s = 0.12$ fm, and total volume $V \sim (1.9\text{fm})^3$. We assume this volume is enough for a first study of doubly-charmed baryons.

The charm quark action used here is similar to the light quark sector and the details are given in Ref. [47]. The η_c meson ground-state was used to determine the bare charm quark mass. By studying the dispersion relation at low momenta, the action is made relativistic. As mentioned in [47], it is expected that the effects due to the absence of dynamical charm quark fields in this calculation will be small.

B. Baryon operators

Following Ref.[49] we construct a large set of baryon operators for doubly-charmed baryons. In summary the construction has two steps: a set of continuum operators with well-defined continuum spin is found and then these operators are subduced to the irreducible representations (irreps) of the octahedral group on the lattice. A set of continuum baryon interpolating operators with well-defined continuum spin are constructed as

$$O^{[J^P]} \sim [\mathcal{F}_{\Sigma_F} \otimes \mathcal{S}_{\Sigma_S} \otimes \mathcal{D}_{\Sigma_D}]^{J^P}, \quad (1)$$

where \mathcal{F} , \mathcal{S} and \mathcal{D} represent flavor, Dirac spin and spatial structure respectively while the subscripts Σ_i specify the permutation symmetry in the respective subspaces. The details of these permutation symmetries and their combinations are given in Refs.[49, 50].

By permutation symmetry, one can argue that the flavor structure of QQq and QQs will be the same as qqq combinations, which are the flavor structures of light Σ baryons. Hence the possible flavor-symmetry structures for doubly charm baryons are totally symmetric (S) in all three flavor labels belonging to the decuplet flavor constructions (10_F) as well as symmetric (MS) and antisymmetric (MA) in the first two flavor labels belonging to the octet flavor constructions (8_F). For the decuplet structure, the flavor labels being symmetric, the remaining spin and spatial part should be combined symmetrically to form an overall symmetric interpolating operator. For the octet structure, the flavor structure being MS and MA, the symmetry in the remaining part of the baryon operator, excluding the color labels, should be MS and MA to form a symmetric interpolating operator.

The spatial- as well as spin-symmetry combinations used are also presented in Ref. [49]. Up to two covariant derivatives are considered and combined so as to transform as orbital angular momentum, L , with maximum accessible values of 0, 1 and 2. The subset of operators formed by considering only the upper two-component of the four-component Dirac-spinor in the Dirac-Pauli representation are labelled non-relativistic, while all other operators are called relativistic. Another subset of operators with $D = 2$ and $L = 1$ in the mixed symmetric and mixed antisymmetric combinations are identified as hybrid operators because of their essential gluonic content; these operators vanish in the absence of a gluon field. In Table II, we show the allowed spin-parity patterns based on non-relativistic quark spinors for up to two covariant derivatives. Note that with the non-relativistic operators, it is not possible to construct a negative-parity state beyond spin $\frac{5}{2}^-$, even with non-local operators using two derivatives. Use of relativistic operators along with non-relativistic ones enable us to extract higher negative-parity states as well as higher excited states. These continuum operators are then subduced to the irreps of the cubic group. The three irreps of the double-valued representations of the octahedral group for half-integer spins are G_1 , G_2 and H . The details of this subduction procedure to obtain the lattice operators was discussed in Ref. [49]. In Table III we show the number of operators that we obtained after subduction and are used for this study. Both the number of positive (g), negative (u) parity operators as well as the number of operators with non-relativistic quark spinors (NR) and with hybrid content are shown in this table.

D	SU(3) _F	S	L	J ^P			
0	8 _F	$\frac{1}{2}$	0	$\frac{1}{2}^+$			
	10 _F	$\frac{3}{2}$	0		$\frac{3}{2}^+$		
<i>N</i> ₀				1	1	0	0
1	8 _F	$\frac{1}{2}$	1	$\frac{1}{2}^-$	$\frac{3}{2}^-$		
		$\frac{3}{2}$	1	$\frac{1}{2}^-$	$\frac{3}{2}^-$	$\frac{5}{2}^-$	
	10 _F	$\frac{1}{2}$	1	$\frac{1}{2}^-$	$\frac{3}{2}^-$		
<i>N</i> ₁				3	3	1	0
2	8 _F	$\frac{1}{2}$	0	$\frac{1}{2}^+$			
		$\frac{1}{2}$	0	$\frac{1}{2}^+$			
		$\frac{1}{2}$	1	$\frac{1}{2}^+$	$\frac{3}{2}^+$		
		$\frac{1}{2}$	2		$\frac{3}{2}^+$	$\frac{5}{2}^+$	
		$\frac{1}{2}$	2		$\frac{3}{2}^+$	$\frac{5}{2}^+$	
	10 _F	$\frac{3}{2}$	0		$\frac{3}{2}^+$		
		$\frac{3}{2}$	2	$\frac{1}{2}^+$	$\frac{3}{2}^+$	$\frac{5}{2}^+$	$\frac{7}{2}^+$
		$\frac{1}{2}$	0	$\frac{1}{2}^+$			
		$\frac{1}{2}$	2		$\frac{3}{2}^+$	$\frac{5}{2}^+$	
		$\frac{3}{2}$	2	$\frac{1}{2}^+$	$\frac{3}{2}^+$	$\frac{5}{2}^+$	$\frac{7}{2}^+$
<i>N</i> ₂				6	8	5	2
2	8 _F	$\frac{1}{2}$	1	$\frac{1}{2}^+$	$\frac{3}{2}^+$		
		$\frac{3}{2}$	1	$\frac{1}{2}^+$	$\frac{3}{2}^+$	$\frac{5}{2}^+$	
	10 _F	$\frac{1}{2}$	1	$\frac{1}{2}^+$	$\frac{3}{2}^+$		
<i>N</i> ₂ (<i>hy</i>)				3	3	1	0

TABLE II: Allowed spin-parity patterns based on non-relativistic quark spinors. For each covariant derivative (D = 0, 1 and 2), the SU(3) flavor, the quark spin *S* and orbital angular momentum *L* are listed followed by the allowed *J^P* values. The total number of operators is listed as *N_i* for derivative *i*. The lower part of the table gives the two-derivative hybrid operators based on non-relativistic quark spinors, as discussed in [51].

	<i>G</i> ₁		H	<i>G</i> ₂	
	<i>g</i>	<i>u</i>	<i>g</i>	<i>u</i>	<i>g</i>
Total	55	55	90	90	35
Hybrid	12	12	16	16	4
NR	11	3	19	4	8

TABLE III: The total number of operators, with covariant derivatives up to two, obtained after subduction to various irreps. The number of non-relativistic (NR) and hybrid operators for each irreps and for both parities are also mentioned.

C. Analysis of baryon correlators : Distillation and variational methods

After constructing a large set of operators for each irrep Λ , we calculate the matrix of correlation functions

$$C_{ij}(t \equiv t_f - t_i) = \langle 0 | O_i(t_f) O_j^\dagger(t_i) | 0 \rangle. \quad (2)$$

between a baryon source at time t_i and sink at time t_f . The *distillation method* [54] provides an efficient means of constructing the large correlation matrices needed for this analysis. For this work, the method was realized by constructing the distillation operator with 64 eigenvectors of the gauge-covariant Laplacian and then correlation functions are computed from 4 time sources. The matrix of correlation functions was then analyzed using the variational method, which proceeds by solving a generalized eigenvalue problem of the form

$$C_{ij}(t) v_j^n = \lambda_n(t, t_0) C_{ij}(t_0) v_j^n, \quad (3)$$

here $C(t)$ is the matrix of correlators at time-slice t , i.e. $C_{ij}(t) = \langle \mathcal{O}_i(t) \mathcal{O}_j(0) \rangle$, $\lambda_n(t, t_0)$ are the *principal correlators* and v_j^n 's are the eigenvectors which determine the overlap of an operator to a particular state. The details of our fitting procedure is given in Ref. [43] and was utilized to extract the excited state spectra of mesons [44–48] as well as of baryons [42, 49–51]. In Figure 1 and Figure 2, we plot some examples of fits to the principal correlators for Ω_{cc} baryons in the H_g irrep and for Ξ_{cc} baryon in the G_{2g} irrep.

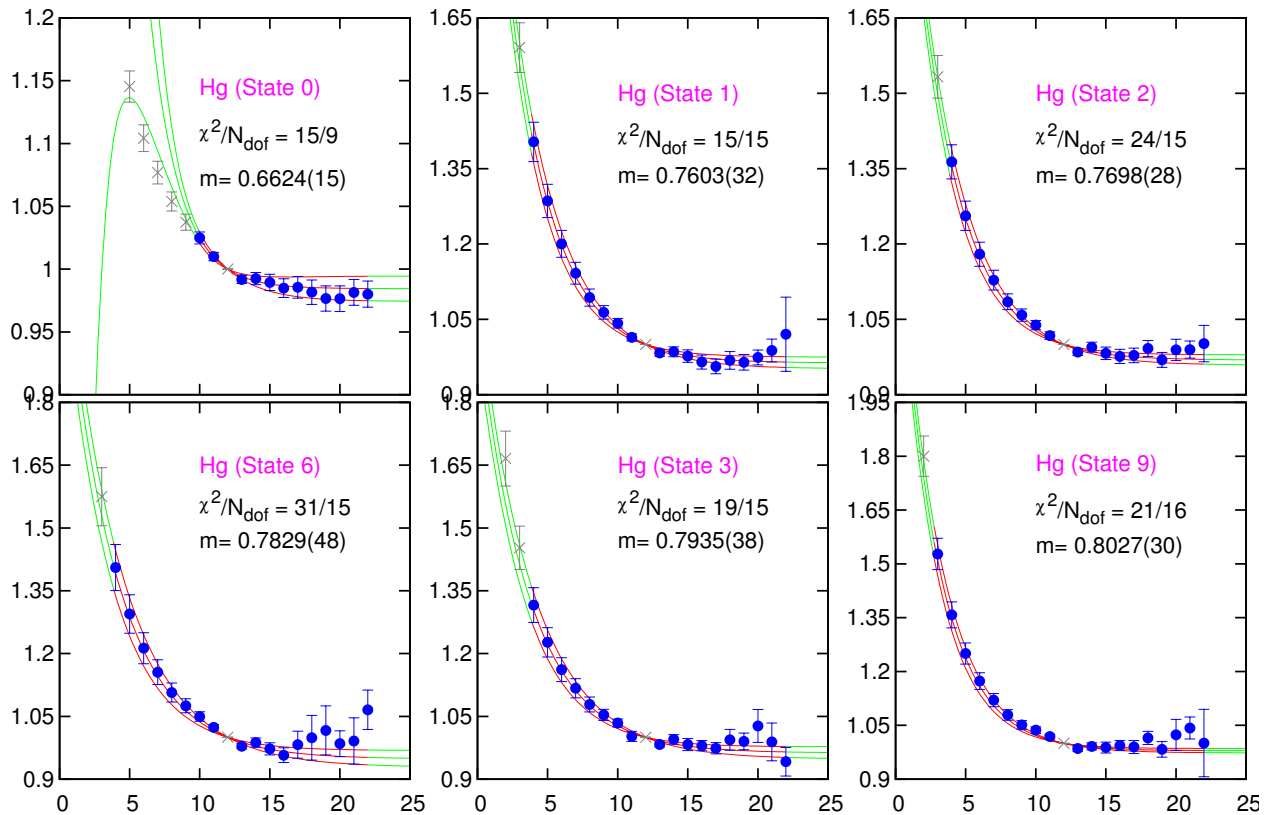


FIG. 1: Principal correlator fits for six states of Ω_{cc} baryons in irrep. H_g that are identified as $J = 3/2^+$. Data points are obtained from $e^{m_n(t-t_0)} \lambda_n(t)$. Fits are carried out using a fitting form $\lambda_n(t) = (1 - A_n)e^{-m_n(t-t_0)} + A_n e^{-m'_n(t-t_0)}$ with three fit parameters, m_n : the state that we are looking for, m'_n : where all other excited states are grouped together, and A_n : which is related to overlap factor. The lines show the fits and one sigma-deviation according with $t_0 = 12$; the grey points are not included in the fits.

D. Rotational symmetry

We constructed operators in the continuum which were then subduced onto the lattice irreps to form lattice operators. This allows us to determine the properties of these states in the continuum with some confidence. Following Refs. [42, 49–51], Figure 3 shows the normalized correlation functions, $C_{ij}/\sqrt{C_{ii}C_{jj}}$, for Ξ_{cc} baryons transforming under H_g and determined at time-slice 5. The normalization ensure diagonal entries are unity and off-diagonal entries are less than 1. Various operators are represented by following abbreviations : non-relativistic (n), relativistic (r), non-hybrid (1) and hybrid (2). There are 90 operators used in this irrep, including operators up to two derivatives. The solid lines divide these operators into spins $\frac{3}{2}$, $\frac{5}{2}$ and $\frac{7}{2}$, and the dashed lines separates operators defined above. As is evident from the figure, the matrix is close to block diagonal implying that there are small correlations between operators subduced from different continuum spins. This suggests that there remains a remarkable degree of rotational symmetry in the matrices of correlation functions obtained for these lattice operators, similar to the light, strange and triply-charmed baryons [42, 50]. Similar block-diagonal matrices of correlation functions are observed in other irreps and for Ω_{cc} baryons as well.

From the correlators one can also identify the flavour mixing between different operators. For example, it is evident

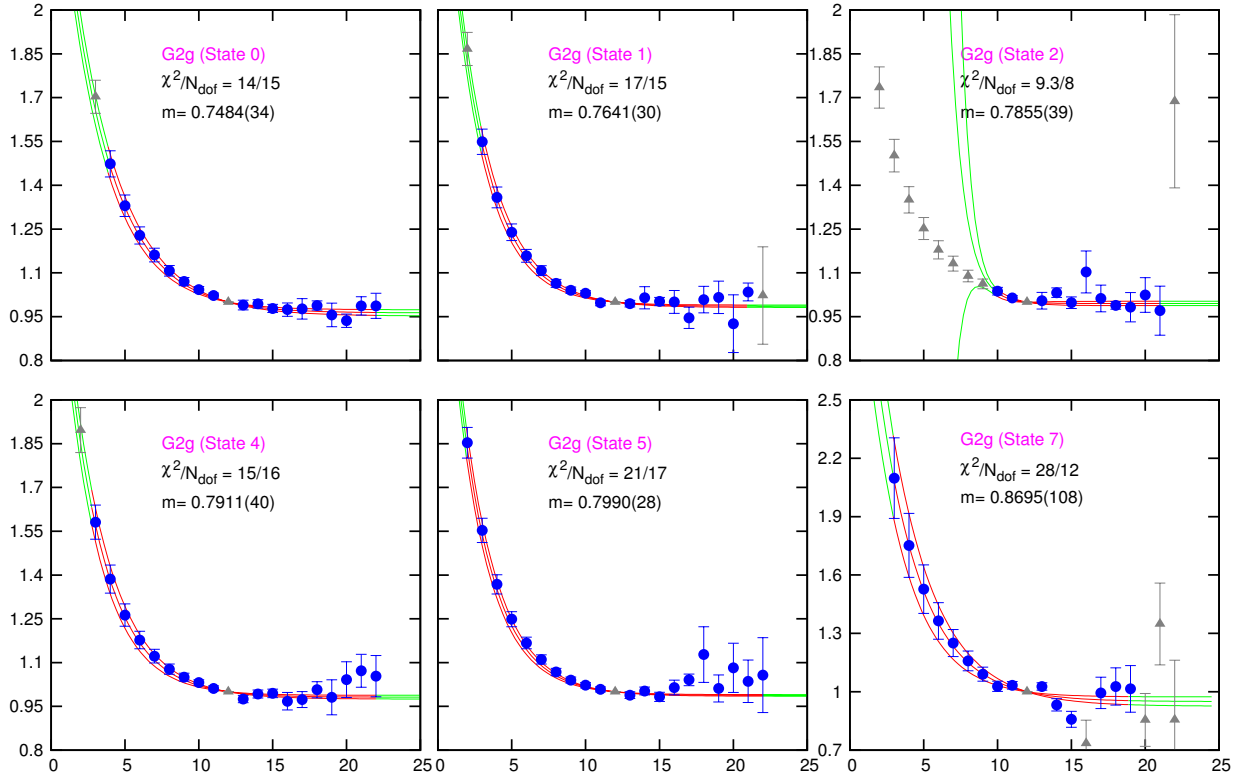


FIG. 2: Same as Figure 2, but for Ξ_{cc} baryons in irrep. G_{2g} .

from Figure 3 that there is strong mixing between relativistic operators belonging to octet and decuplet. However, this flavour mixing is less evident for non-relativistic operators. As was observed in our previous study on triply-charmed baryons [42], we found that there are additional suppression in mixing for non-relativistic operators with a given J , but with different L and S , compared to those with the same J , as well as the same L and S . However, this suppression is not present for relativistic operators. On the contrary, in most of the cases involving relativistic operators, we found that mixings are comparable for operators with given J , but with different L and S to those of operators with the same J , as well as same L and S .

1. Continuum spin identification

One main difficulty of lattice calculations of spectra is the identification of the spin of an extracted state at finite lattice spacing, particularly for the state onto which various operators from different irreps contribute. In Ref. [43] a well defined procedure is adopted for spin identification by using the overlap factor. The *overlap-factors* of an operator O_i to a state n are $Z_i^n \equiv \langle n|O_i^\dagger|0\rangle$ which can be shown [43] to occur in the spectral decomposition of the matrices of the correlation functions as,

$$\text{corr}C_{ij}(t) = \sum_n \frac{Z_i^{n*} Z_j^n}{2m_n} e^{-m_n t}. \quad (4)$$

One can use the orthogonality for the eigenvectors $v^{n\dagger} C(t_0) v^m = \delta^{n,m}$ to show that the overlap factors can be obtained from the eigenvectors using the relation

$$Z_i^n = \sqrt{2m_n} e^{m_n t_0/2} v_j^n C_{ji}(t_0). \quad (5)$$

In Figure 4, we show an array of histograms of the normalized overlap factors, $\tilde{Z} = \frac{Z_i^n}{\max_n [Z_i^n]}$, of a few operators

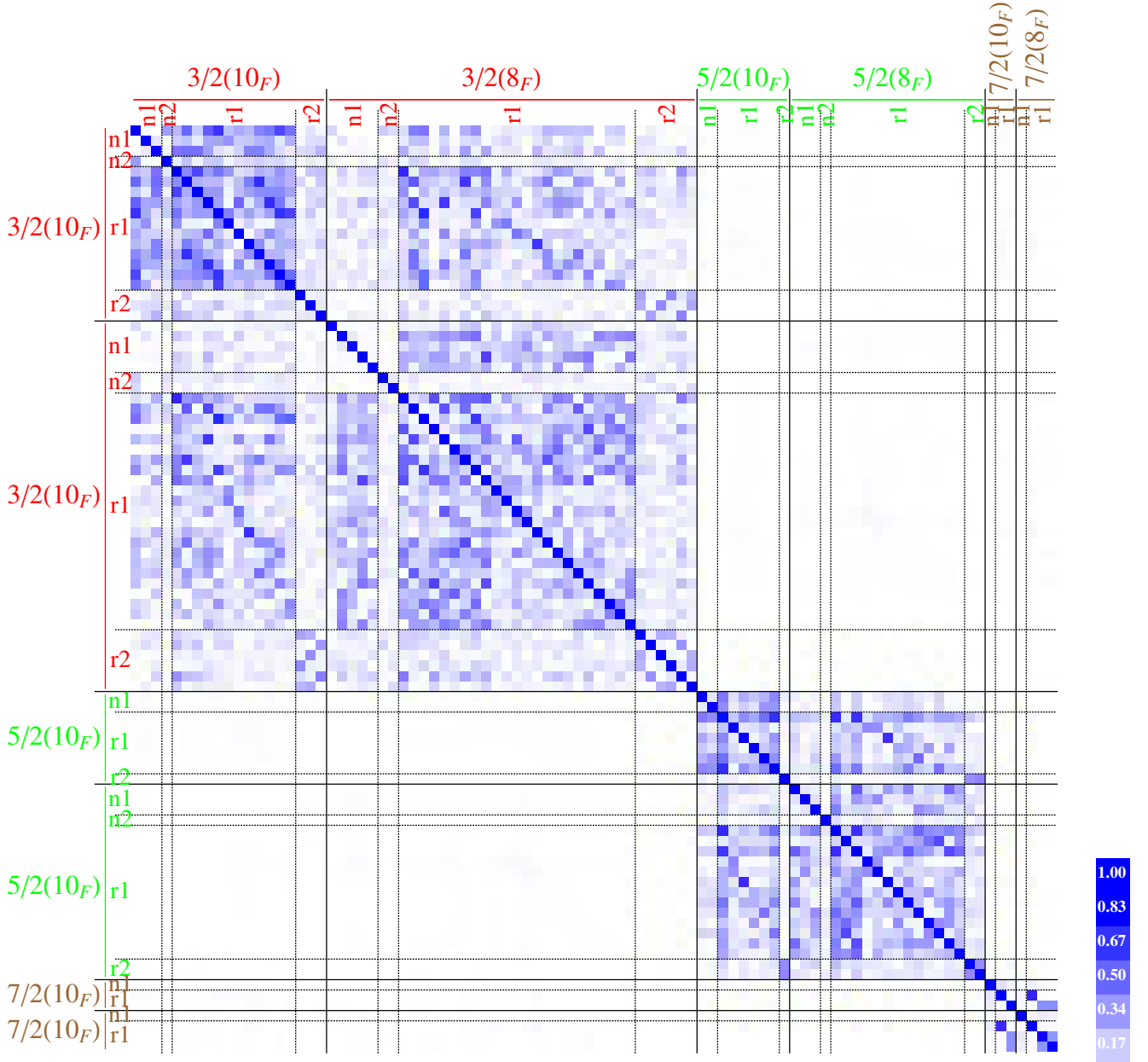


FIG. 3: The normalized correlation matrix, $C_{ij}/\sqrt{C_{ii}C_{jj}}$, at $t/a_t = 5$ are shown for Ξ_{cc} baryons in the H_g irrep., according to the darkness scale at the side. The operators are ordered such that those subduced from spin 3/2 appear first followed by spin 5/2 and then spin 7/2. The correlation matrix is observed to be mostly block diagonal in terms of spins which signifies the rotational symmetry on our lattice. There is significant mixing between octet (8_F) and decuplet (10_F) operators which is not present in the corresponding plot for light quark $\Sigma(uus)$ having same operator structures (see figure 2 of Ref.[50]). This signifies that the $SU(3)$ flavor symmetry is badly broken for doubly-charmed Ξ_{cc} baryons. Non-relativistic (n), relativistic (r), non-hybrid (1) and hybrid (2) operators are also identified for each of those spins. The strength of flavor mixing is maximum between relativistic operators (r), while for non-relativistic operators this mixing is relatively mild.

onto some of the spin identified lower-lying states in each of the lattice irreps. The normalization $\tilde{Z} = \frac{Z_i^n}{\max_n[Z_i^n]}$ is such that the largest overlap factor of that operator across all states is unity.

As in Ref.[50], a “matrix” plot of the overlap factors can be used to depict the dominant contribution to the low-lying states from each operator. As examples, Figure 5 and Figure 6 show such plots of the normalized overlap factors, Z_i^n , of an operator i to a given state n , as defined by eq. (5), for Ξ_{cc} and Ω_{cc} respectively. All values of Z_i^n are normalized as above. Figure 5 shows that state 0, the ground state, and excited states 1, 2, 3, 4, 9, 12 and 15 are

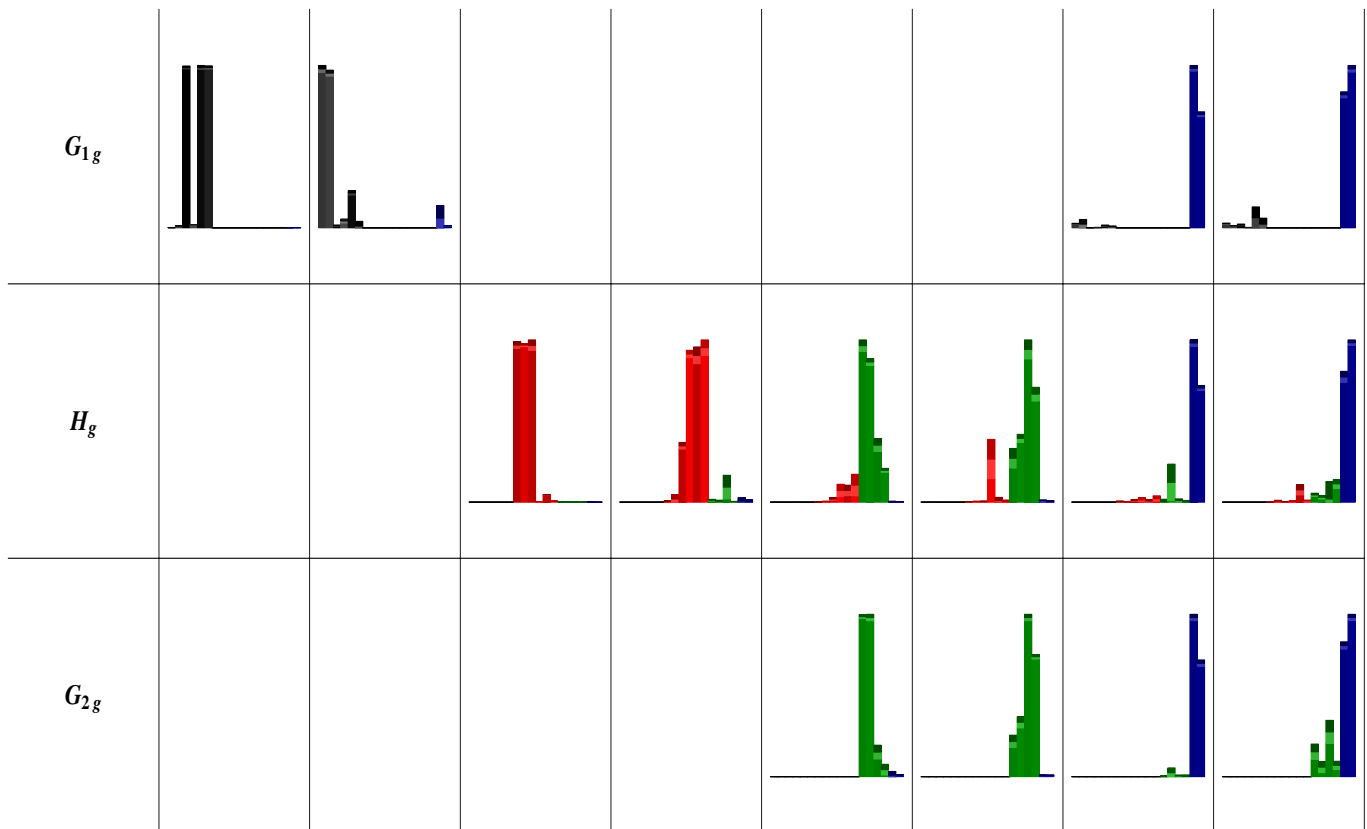


FIG. 4: Histogram plot showing normalized overlap factor, \tilde{Z} , of a few operators onto some of the lower-lying states in each of the lattice irreps. \tilde{Z} 's are normalized according to $\frac{Z_i^n}{\max_n[Z_i^n]}$, so that the largest value for that operator across all states is equal to unity. Top row is for irrep G_{1g} , middle one is for H_g , and the bottom one is for G_{2g} irrep. Black bars correspond to spin-1/2 operators, red for spin-3/2, green for spin-5/2 and blue represents spin-7/2 operators. Lighter and darker shades on the top of every bar represent the one sigma statistical uncertainty.

naturally identified as $J^P = \frac{3}{2}^+$ states while states 5, 7, 8, 10 and 13 are identified as $J^P = \frac{5}{2}^+$ states and similarly, states 11 and 14 can be identified as $J^P = \frac{7}{2}^+$ states. However, in order to confirm the reliability of the identification of a state with a given spin greater than $3/2$ we compare the magnitudes of overlap factors of a particular operator from different irreps. This will be discussed later. These plots help us to identify the structure of a state from the types of operators which construct it. For example, in Figure 5, the spin-3/2+ ground state has predominant overlaps from the non-relativistic non-hybrid as well as relativistic non-hybrid type operators. Similarly, the states 11 and 14, which are identified as $\frac{7}{2}^+$ states, have predominant overlaps to non-relativistic non-hybrid operators. Strong hybrid content was observed for a number of states by identifying their strong overlaps with hybrid interpolating operators.

To identify the spin parity of a state we followed the same method detailed in [43] and used for light mesons [44–46], baryons [49, 50], charm mesons [47] as well as heavy-light mesons [48] calculations. To identify a spin that subduces into a single irrep is relatively straightforward and studying the overlap factors used in histogram and matrix plots we can identify spin- $\frac{1}{2}$ and spin- $\frac{3}{2}$ states. For spin- $\frac{5}{2}$ and spin- $\frac{7}{2}$ states, which are subduced into multiple irreps overlap factors from different irreps must be compared. As the continuum limit is approached, the factors of a given continuum operator to a particular state obtained from various subduced irreps should be the same. For a fine lattice spacing these overlap factors should thus be close to each other. For example, the spin-7/2 continuum operator, $(3/2^+)_{1,S} \otimes D_{L=2S}^{[2]}$, can be subduced to irrep G_{1g} , H_g as well as to G_{2g} . This near degeneracy of overlap factors can be used to identify this state as spin- $\frac{7}{2}^+$ state. In Figure 7 we compare a selection of Z -values for states conjectured to be $J = \frac{5}{2}^+$ (top two plots), $\frac{7}{2}^+$ (middle two plots), $\frac{5}{2}^-$ (bottom left) and $\frac{7}{2}^-$ (bottom right) which appear over multiple lattice irreps. The continuum operators considered are noted along the lower edge of each plot. Z -values obtained for a given operator but from different irreps are found to be consistent with each other which helps us to identify the spin of these given states.

After identifying the spin of a state with matching overlap factors we check whether the energy of this state

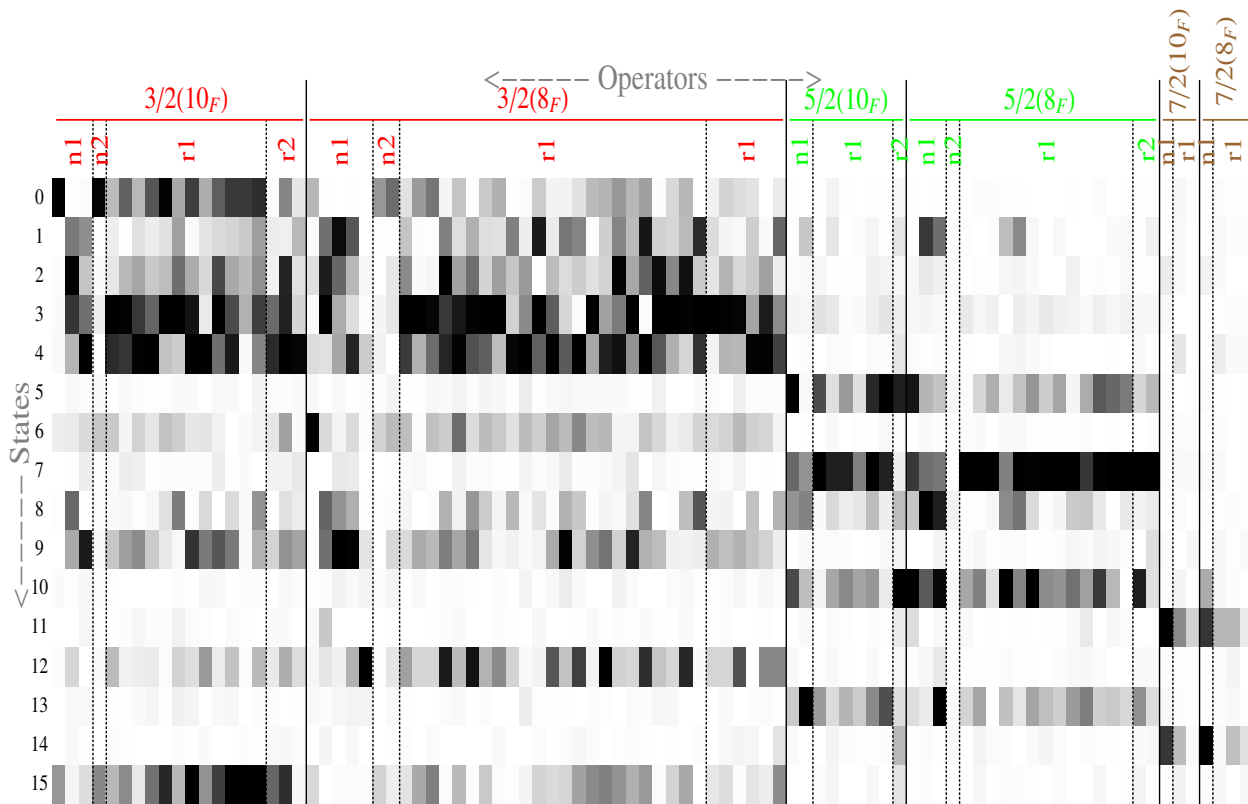


FIG. 5: “Matrix” plot of the normalized overlap factor, \tilde{Z}_i^n , of an operator i to a given state n , as defined by eq. (5). \tilde{Z}_i^n are normalized according to $\frac{Z_i^n}{\max_n[Z_i^n]}$, so that for a given operator the largest overlap across all states is unity. This plot corresponds to the extracted states of Ξ_{cc} , in the H_g irrep. Darker pixels indicate larger values of the operator overlaps as in Figure 3. Various type of operators, for example, non-relativistic (n) and relativistic (r) operators, as well as non-hybrid (1) and hybrid (2) operators are indicated by column labels. In addition, the continuum spins of the operators are shown by 3/2, 5/2 and 7/2. State 0, the ground state, and excited states 1, 2, 3, 4, 9, 12 and 15 could be identified as $J^P = \frac{3}{2}^+$ states by the overlap to various types operators according to pixel strengths. States 5, 7, 8, 10 and 13 could be identified as $J^P = \frac{5}{2}^+$ states; similarly, states 11 and 14 could also be identified as $J^P = \frac{7}{2}^+$ states.

determined over different irreps also matches. To achieve this check, the corresponding principal correlators across the irreps are simultaneously fit to a single energy. In Figure 8, these joint fits are shown for the principal correlators obtained from three different irreps for a spin-7/2⁺ state (top plot) and from two different irreps for a spin-5/2⁺ state (bottom plot).

III. RESULTS

In this section, our results for the doubly-charmed baryons spectra with spins up to $\frac{7}{2}$ and with both parities are presented in terms of energy splittings. In general, this tends to reduce systematic uncertainties in lattice calculations, including those from the scale setting procedure used. For this work, the charm quark mass parameter in the lattice action was determined by ensuring the physical value and lattice estimate of the η_c meson mass [47] agreed, once the lattice spacing is determined using the Ω -baryon. The η_c meson has the same number of charm quarks as the doubly-charmed baryons. Hence, we show the spectra of Ξ_{cc} and Ω_{cc} baryons with the mass of the η_c meson subtracted. These energy splittings expose the binding energies of the extra light and strange quarks inside these baryons. A few energy splittings such as the hyperfine splittings between the extracted states are also computed.

As mentioned earlier, the experimental status of doubly heavy baryon discovery is uncertain. It is thus important to compare the ground state spectra of the two doubly heavy baryon discovery is uncertain. It is thus important to compare the ground state spectra of the two doubly heavy baryons obtained from different calculations. In Figure 10, we show the ground state results of $J^P = \frac{1}{2}^+, \frac{3}{2}^+, \frac{1}{2}^-$ and $\frac{3}{2}^-$ of Ξ_{cc} baryons, obtained in this work, along with

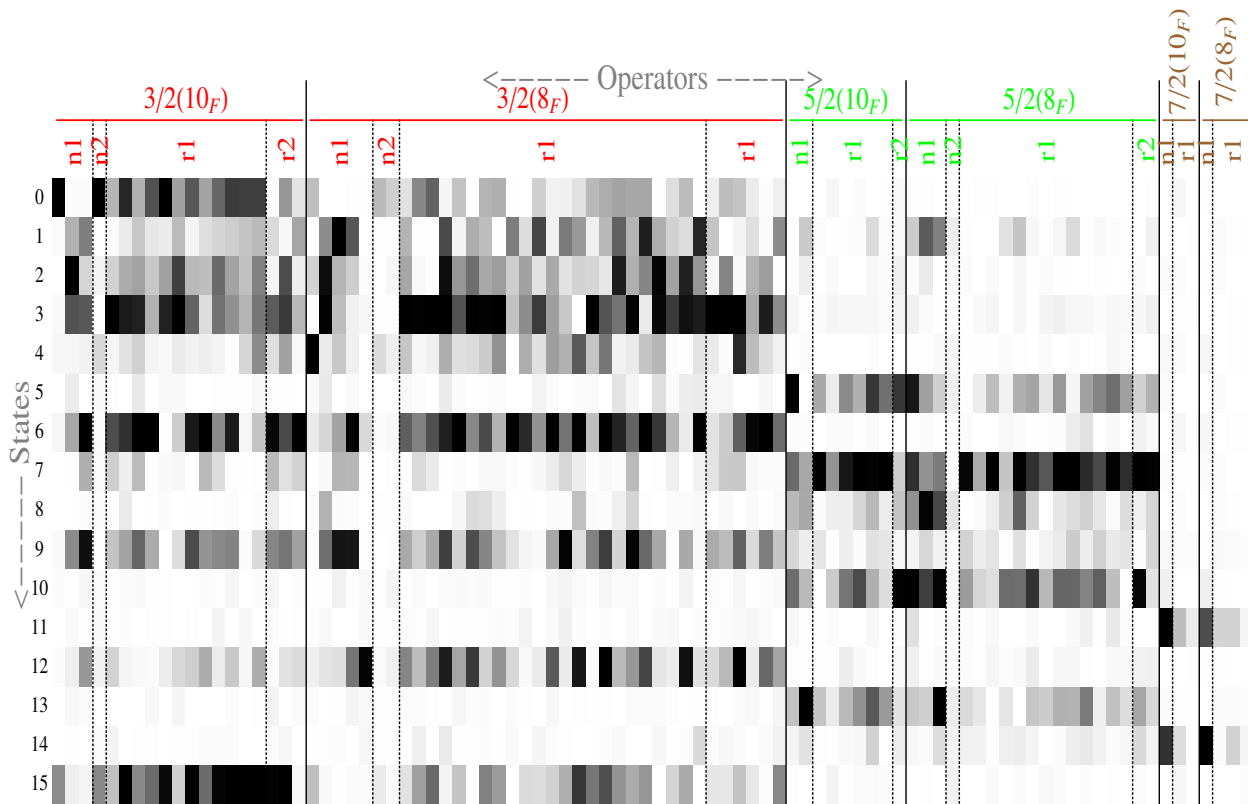


FIG. 6: Same as Figure 5, but for Ω_{cc} baryons in the irrep H_g .

the only experimental (SELEX) result and other lattice as well as various model results. In Figure 9, we show similar results for Ω_{cc} baryons. Our results are at pion mass 391 MeV, results for ETMC [38], PACS-CS [41], Bali *et. al* [40], and Briceno *et. al* [37] are extrapolated to the physical pion mass, while ILGTI [39] results are at pion mass 390 MeV. While the lattice spacing in the temporal direction (a_t) for this work is 0.0351 fm, for ETMC, $a_t = 0.056$ fm, for PACS-CS, $a_t = 0.0899$ fm, for Bali *et. al*, $a_t = 0.0795$ fm and for ILGTI, $a_t = 0.0582$ fm. Results for Briceno *et. al* are extrapolated to the continuum limit.

In Figure 11 and Figure 12 we show the spin identified full spectra, up to $J = \frac{7}{2}$ extracted from our lattices of Ξ_{cc} and Ω_{cc} baryons, respectively. The states inside the magenta boxes are those with relatively large overlap onto non-relativistic operators and the states with thick borders corresponds to the states with strong hybrid content as defined in Ref. [51].

Note that in the lowest two positive parity bands and the lowest negative parity band, the number of states for each spin agrees with the expectation shown in Table II. That table gives the number of allowed quantum numbers by $SU(6) \times O(3)$ symmetry for operators with up to two derivatives (D). For $J^P = \frac{1}{2}^+$ and $J^P = \frac{3}{2}^+$, the number of allowed quantum numbers is 7 (1 from D = 0 and 6 from D = 2) and 9 (1 from D = 0 and 8 from D = 2) respectively. For other positive parity quantum numbers with $J^P = \frac{5}{2}^+$ and $\frac{7}{2}^+$ these numbers are 5 and 2 respectively. The left sides of Figure 11 and Figure 12 show positive parity states. The numbers of states in the lowest two bands (first two and inside box) match exactly with the allowed quantum numbers mentioned above. Note that while we use the full set including both non-relativistic and relativistic operators not in Table II, we still obtain the same number of states allowed with only non-relativistic operators. Similarly, for negative parity with $J^P = \frac{1}{2}^-$, $\frac{3}{2}^-$, $\frac{5}{2}^-$, $\frac{7}{2}^-$, the allowed number of quantum numbers are 3, 3, 1 and 0, respectively. On the right sides of Figure 11 and Figure 12, the lowest band (inside box) also has exactly the same number of states. This agreement of the number of low lying states between the lattice spectra obtained in this work and the expectations based on non-relativistic quark spins implies a clear signature of $SU(6) \times O(3)$ symmetry in the spectra. Such $SU(6) \times O(3)$ symmetric nature of spectra was also observed in Ref. [42, 50]. Note there are no negative parity spin-7/2 state in that table and the negative parity spin-7/2 state is obtained from the inclusion of relativistic operators. We are also able to identify one state with strong overlap onto a hybrid operator. Though there are more quantum numbers accessible with the operators

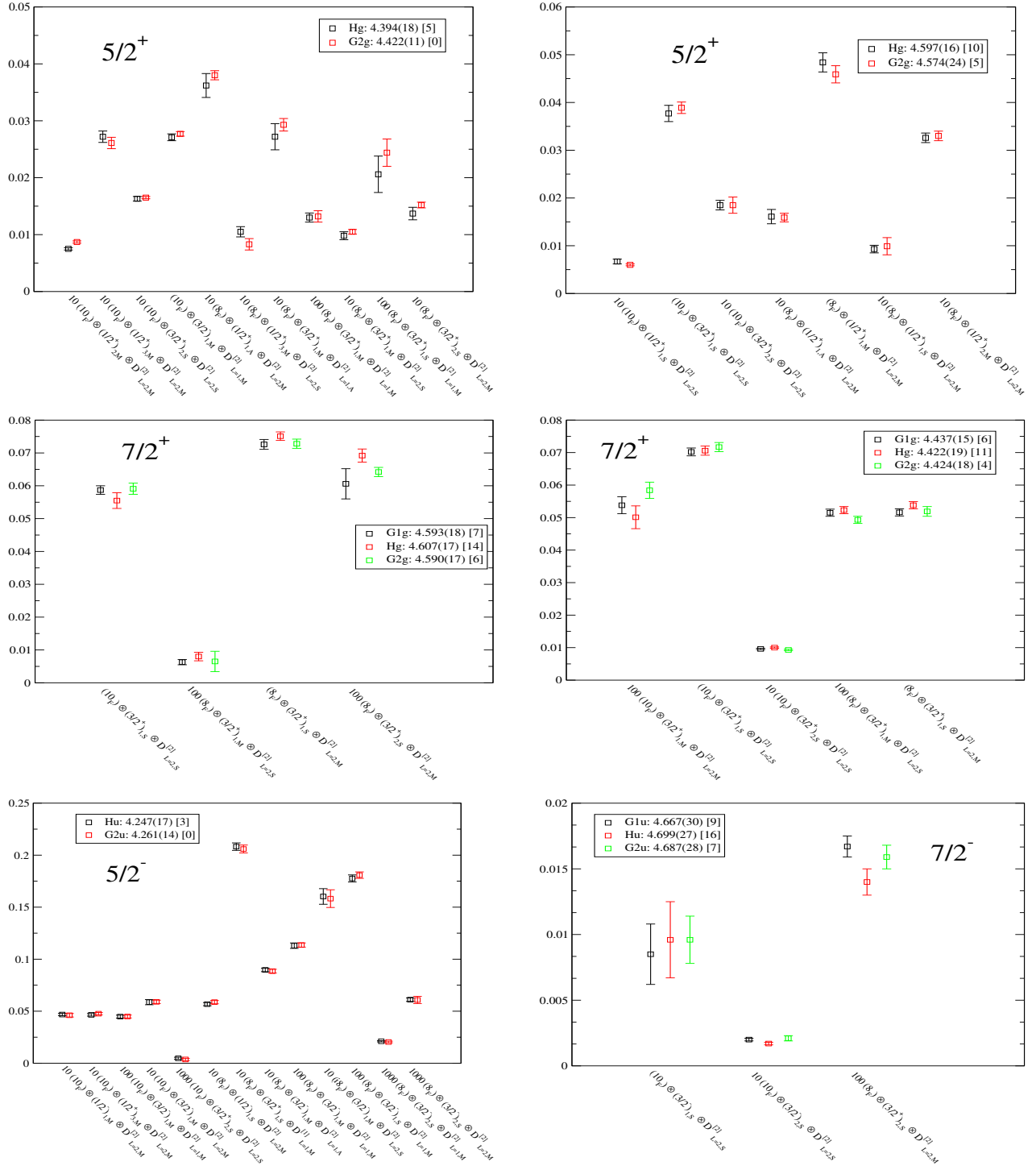


FIG. 7: A selection of Z -values for states conjectured to be $J = \frac{5}{2}^+$ (top two plots), $\frac{7}{2}^+$ (middle two plots), $\frac{5}{2}^-$ (bottom left) and $\frac{7}{2}^-$ (bottom right). The operators used are mentioned at the bottom of each plot. Z -values obtained for a given operator, but from different irreps, are found to be consistent.

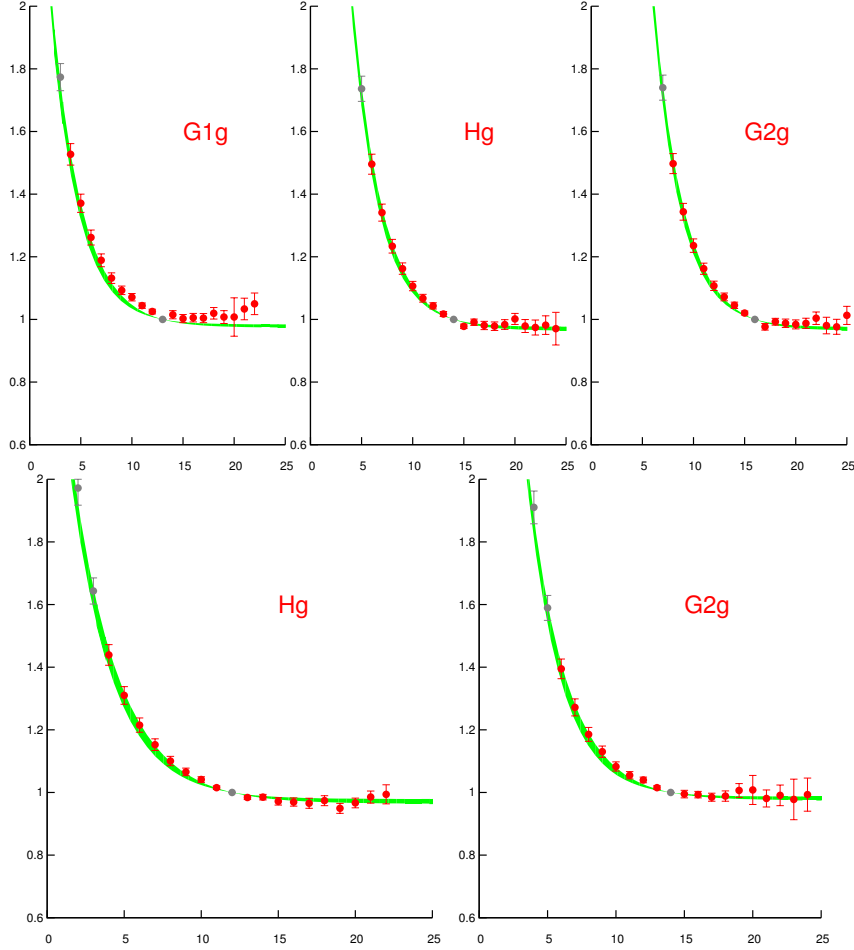


FIG. 8: Joint fit of the three principal correlators : top figures – for a representative spin- $\frac{7}{2}^+$ state from three different irreps, and bottom figures – for a spin- $\frac{5}{2}^+$ state from two different irreps. Joint fits with $\chi^2/dof \sim 1.9$ (for both cases) provide the masses of these states.

in Table II with hybrid structures, we could not clearly identify those. This is because, as noted in Ref. [50], it is not meaningful to interpret the higher excited states in terms of $SU(6) \times O(3)$ symmetry.

Figure 13 shows the extracted spectra with a different subtraction. The doubly-charmed Ξ_{cc} baryons have two charm quarks and one light quark. On the other hand, D meson has one charm quark and one light quark. The computed energy splittings between Ξ_{cc} and the ground state of D meson are shown in Figure 13. In the same figure the energy splittings between Ω_{cc} and the ground state of D_s are shown. For each spin, the left column indicates splittings of $\Xi_{cc} - D$ while the right column shows $\Omega_{cc} - D_s$ splittings. The inset at the top figures shows the positive parity ground states of spin-1/2 and spin-3/2 baryons. Results for D and D_s mesons are taken from Ref. [48]. By subtracting the D and D_s meson masses from Ξ_{cc} and Ω_{cc} baryons we effectively leave only the energy of the excitation of a single charm quark in both cases. One would thus naively expect that both spectra will be equivalent. This is almost true for the lowest state in each spin parity channel, except for negative parity spin-7/2 state, as shown in Figure 13. That state is obtained from relativistic operators and it is expected that such naive expectation may not hold there. This is also seen for the excited states where the contribution from relativistic operators is much larger.

As in our previous studies in charmonia [47], charmed-strange mesons [48] and triply-charmed baryons [42], the systematic uncertainty due to $\mathcal{O}(a)$ discretisation artefacts was investigated in another calculation in which the spatial clover co-efficient was boosted from the tree-level $c_s = 1.35$ to $c_s = 2$. At this value our extracted hyperfine splitting was found to be physical [47]. The mass splittings were found to differ by around 40-45 MeV between the two calculations. In this study also we found a similar mass difference between two calculations, indicating an equivalent scale for the uncertainties in this calculation.

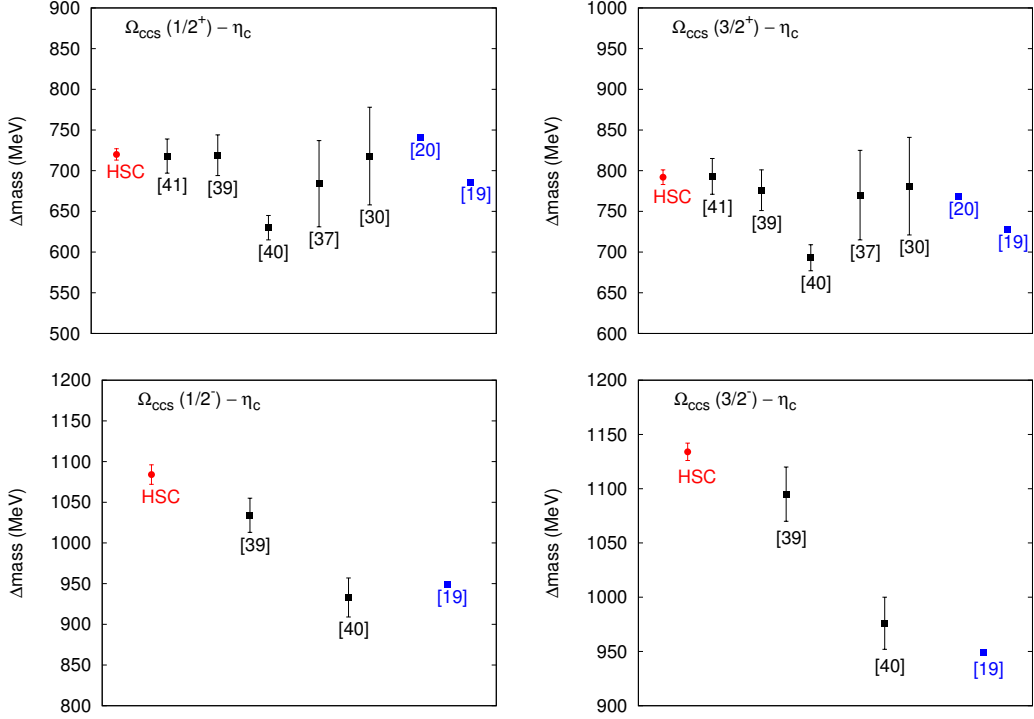


FIG. 9: Ground state masses of spin-1/2 and spin-3/2 doubly-charmed Ω baryons as a splitting from η_c meson mass. Our results are shown by the red filled circle (HSC). Other lattice as well as model results are also shown.

A. Energy Splittings

The energy splittings between various excitations in a spectrum provide important information about the nature of interactions needed to excite those states. The energy splittings also provide inputs for building models to describe these states successfully. In Figure 14 we show energy splittings of the ground states of each spin parity channel from the lowest state in that parity channel. For the positive parity, the lowest state is $J^P = \frac{1}{2}^+$ and for negative parity the lowest state is $J^P = \frac{1}{2}^-$. It is interesting to note that both for Ξ_{cc} and Ω_{cc} this splittings are almost same. This indicates that the interquark interactions, which are responsible for these splittings, are similar in these two different type of baryons.

The most notable spin dependent baryon energy splitting to consider is the hyperfine splittings between $\frac{3}{2}^+$ and $\frac{1}{2}^+$ states, for example splitting between Δ and nucleon. For doubly-charmed baryons we also compute this splitting and show in Figure 15 for Ξ_{cc} (left plot) and Ω_{cc} (right plot) baryons. Our results (red circles) are compared with other lattice results (blue squares) as well as with various model results. Note our results for Ξ_{cc} are for pion mass 391 MeV. Results for ETMC [38], PACS-CS [41], Bali *et. al* [40], and Briceño *et. al* [37] are extrapolated to the physical pion mass, while ILGTI [39] results are at pion mass 390 MeV.

In Figure 16 we compare these hyperfine splittings for Ξ_{cc} and Ω_{cc} baryons as a function of quark mass. In the x -axis of that figure we use the square of the pseudoscalar meson mass (m_{ps}) while y -axis shows hyperfine splittings at those pseudoscalar meson masses. Along with Ξ_{cc} and Ω_{cc} we also show splittings between spin- $\frac{3}{2}$ and spin- $\frac{1}{2}$ states of Ω_{ccc} baryon. The later spin dependent splitting is not hyperfine in nature as both of them are of decuplet type. As in Ref. [42], for the positive parity Ω_{ccc} baryons we take the spin-orbit splitting between $E_3(\frac{3}{2}^+)$ and $E_0(\frac{1}{2}^+)$ states which have same L and S values. For the negative parity Ω_{ccc} baryons we take spin-orbit splitting between $E_0(\frac{3}{2}^-)$ and $E_0(\frac{1}{2}^-)$ states which also have same L and S values.

In Ref. [42] we evaluated energy splittings between triply-flavoured baryons¹ and studied their quark mass depen-

¹ by triply-flavoured baryons, we mean Δ , Ω , Ω_{ccc} and Ω_{bbb} baryons.

dence. It was observed that various splittings decrease significantly with quark masses. Following heavy quark effective theory one can expand the mass of a heavy hadron, with n heavy quarks, as $M_{H_{nq}} = nM_Q + A + B/m_Q + \mathcal{O}(1/m_Q^2)$ [55]. With that expectation, we fitted various energy splittings of triply-flavoured baryons with a form $a + b/m_{ps}$, with m_{ps} the pseudoscalar meson mass, and obtained good fits. Motivated by that, here we also fit similar energy splittings for doubly-charmed baryons. There is a however a difference for doubly-charmed baryons because to show quark mass dependence one needs to use triply-charmed baryons data also. For the triply-flavoured baryons in Ref. [42], states at different quark masses are obtained from the same operators and so are simple to compare. However, in this work, doubly- and triply-charmed baryons are not obtained from the same operators except for positive parity spin 3/2 and spin-7/2 states. We thus consider energy splittings only for these states. More specifically, we calculate the following energy splittings: $\Xi_{cc}^*(ccu) - D_u(\bar{c}u)$, $\Omega_{cc}^*(ccs) - D_s(\bar{c}s)$ and $\Omega_{ccc}^*(ccc) - \eta_c(\bar{c}c)$, and $\Xi_{cc}^*(ccu) - D_u^*(\bar{c}u)$, $\Omega_{cc}^*(ccs) - D_s^*(\bar{c}s)$ and $\Omega_{ccc}^*(ccc) - J/\psi(\bar{c}c)$ and plot in Figure 17. As in Ref. [42], we fit these splittings to the form $a + b/m_{ps}$ and obtain reliable agreement. Energy splittings from vector mesons are also fitted with a constant. We emphasize that energy splittings at very light quark masses should not be calculated using the above form, which is valid only for heavy quarks.

It is interesting to note that one can extrapolate the fitted results to the bottom mass to obtain the energy splittings of $\Omega_{ccb}^*(\frac{3}{2}^+) - B_c$ and $\Omega_{ccb}^*(\frac{3}{2}^+) - B_c^*$ at the mass of B_c meson. The difference between these two quantities yields the mass splitting of $B_c^* - B_c$. Using this, we obtain the mass splitting of $B_c^* - B_c$ as 80 ± 8 MeV (fitting with a form $a + b/m_{ps}$) and 76 ± 7 MeV (fitting with a constant term). This result agrees very well with those obtained by potential models [56]. It does not however agree with other lattice QCD prediction [57–59] which provide much lower values. It will be interesting to study the effects of the lattice cut-off on the hyperfine splittings of these hadrons with the possibility of future discovery of B_c^* meson. Only one charmed-bottom meson has been discovered so far [1]. Assuming it as a pseudoscalar meson with mass 6277 MeV and using the extrapolated value of $\Omega_{ccb}^*(\frac{3}{2}^+) - B_c$, we empirically predict the mass of $\Omega_{ccb}^*(3/2^+)$ to be 8050 ± 10 MeV which is consistent with the results from various models [20, 60, 61] and a recent lattice calculation [?].

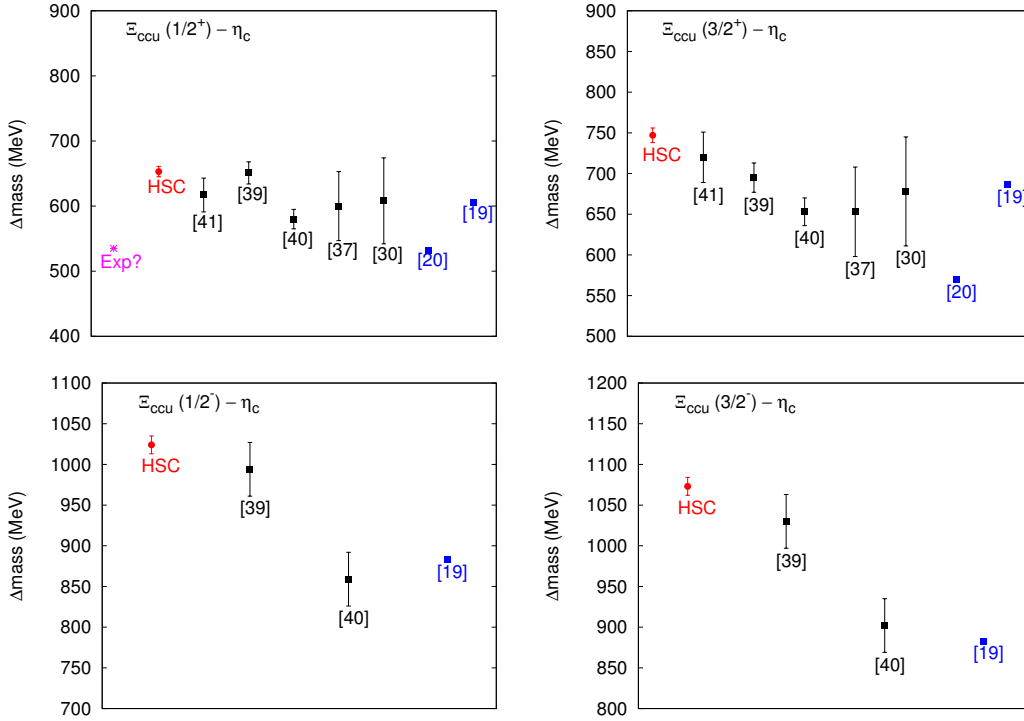


FIG. 10: Ground state masses of spin-1/2 and spin-3/2 doubly-charmed Ξ_{cc} baryons as a splitting from η_c meson mass. Our results are shown by the red filled circle (HSC). Our u quark mass is not physical and at pion mass 392 MeV, results for ETMC [38], PACS-CS [41], Bali *et. al* [40], and Briceno *et. al* [37] are extrapolated to the physical pion mass, while ILGTI [39] results are at pion mass 390 MeV and 340 MeV respectively.

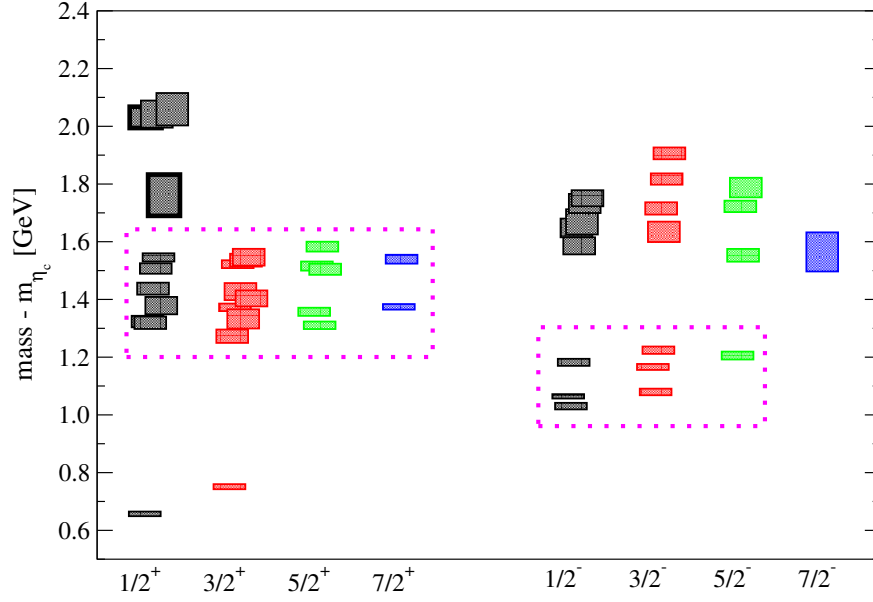


FIG. 11: Spin identified Ξ_{cc} baryon spectra for both parities and with spin up to $7/2$. Energy splittings of the Ξ_{cc} baryons from the mass of m_{η_c} meson, which has same number of charm quarks, are shown here. The states inside the pink boxes are those with relatively larger overlap to non-relativistic operators and the states with thick borders corresponds to the states with strong hybrid content. The number of states inside these boxes matches with the expectations based on non-relativistic quark spins, as shown in Table II. This agreement of the number of low lying states between the lattice spectra obtained in this work and the expectations based on non-relativistic quark spins implies a clear signature of $SU(6) \times O(3)$ symmetry in the spectra.

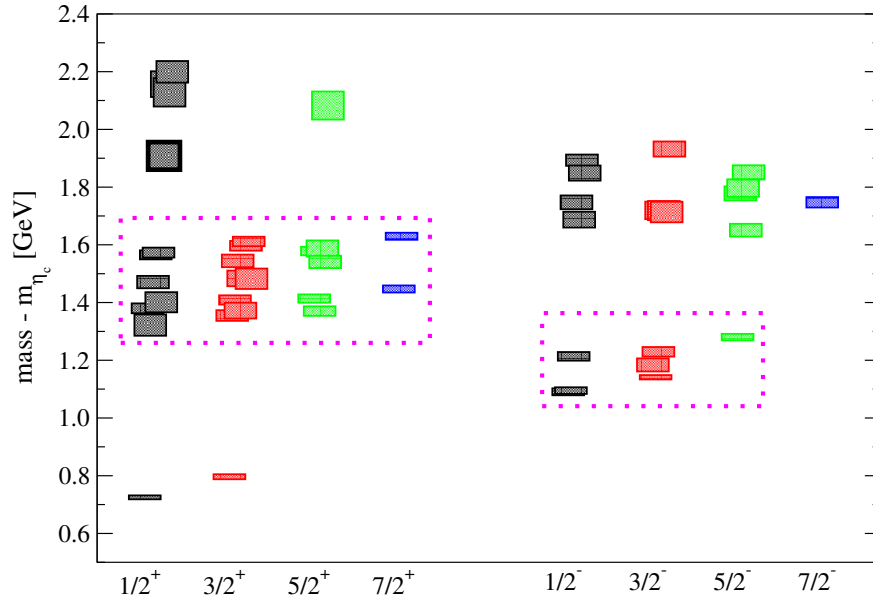


FIG. 12: Spin identified spectra of Ω_{cc} baryons for both parities and with spin up to $7/2$. Energy splittings of the Ω_{cc} states from the mass of η_c meson, which has same number of charm quark, are shown here. All other details are same as in Figure 10.

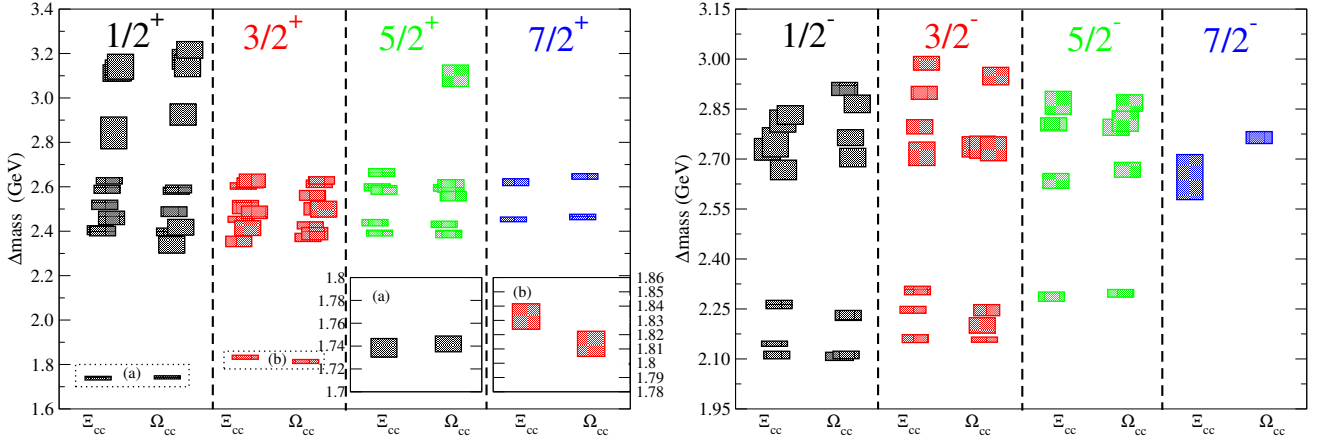


FIG. 13: Energy splittings of Ξ_{cc} and Ω_{cc} baryons from D and D_s mesons, respectively. Splittings for the positive parity baryons are in the left plot and those for negative parity baryons are shown in the right plot. For each spin, left column is for splittings of $\Xi_{cc}(ccu)$ baryons from the ground state $D(cu)$ meson and the right column is for splittings of $\Omega_{cc}(ccs)$ baryons from the ground state $D_s(cs)$ meson. The inset at the top figures are for the positive parity ground states of spin-1/2 and spin-3/2 baryons. Results for D and D_s mesons are taken from Ref. [48].

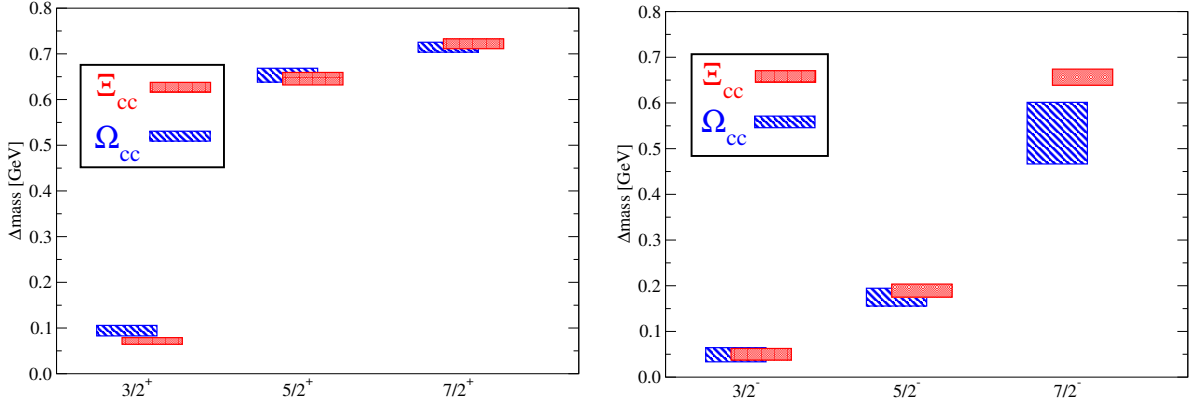


FIG. 14: Energy splittings (in units of GeV) of the ground states of each spin parity channel from the lowest state in that parity channel. Splittings for Ξ_{cc} are shown with red color rectangle and those of Ω_{cc} are represented by blue color shredded rectangle. For the positive parity, the lowest state has $J^P = \frac{1}{2}^+$ and for the negative parity the lowest state has $J^P = \frac{1}{2}^-$.

IV. CONCLUSIONS

In this work, results from the first non-perturbative calculation on the excited state spectroscopy of the doubly-charmed baryons with spin up to 7/2 are presented. We performed our calculations using lattice QCD with dynamical $2 + 1$ flavours clover quarks on anisotropic lattices. There is no clear experimental observation to date of a doubly-charmed baryon. It is important for theory to determine if various model results using quark-diquark symmetry or otherwise, can be tested with a non-perturbative method for these systems for which the interaction is governed by two widely separated scales. Our extensive study of doubly charmed baryons has made a first attempt to connect possible experimental and theoretical studies.

We employ a large basis of creation operators and use the distillation technique to calculate the doubly-charmed baryon correlation functions. A variational fitting method was employed to extract the spectrum. We observe approximate rotational symmetry for these operators at the scale of hadrons. Having realized a good rotational symmetry we determine the overlap factors, as in previous studies [42–51]. We are able to extract states reliably with spin up to 7/2 and also studied the mixing between various operators.

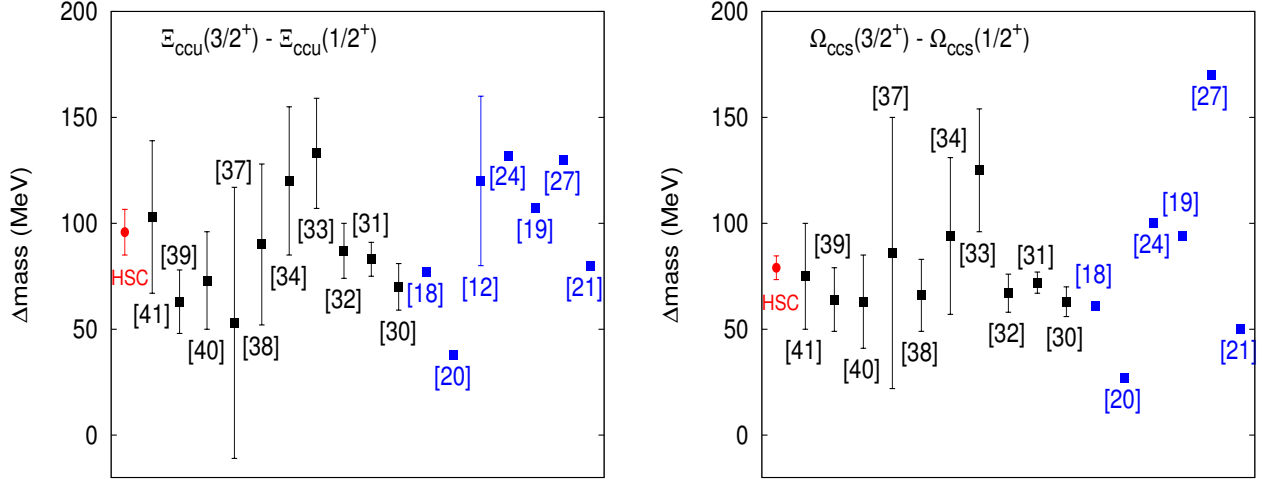


FIG. 15: Hyperfine mass splittings between spin- $\frac{3}{2}^+$ and spin- $\frac{1}{2}^+$ states of Ξ_{cc} (left plot) and Ω_{cc} (right plot) baryons are compared for various lattice and model results. Our results are shown by red filled circle (HSC). Results from this work are at pion mass 392 MeV, results for ETMC [38], PACS-CS [41], Bali *et. al* [40], and Briceno *et. al* [37] are extrapolated to the physical pion mass, while ILGTI [39] results are at pion mass 390 MeV and 340 MeV respectively.

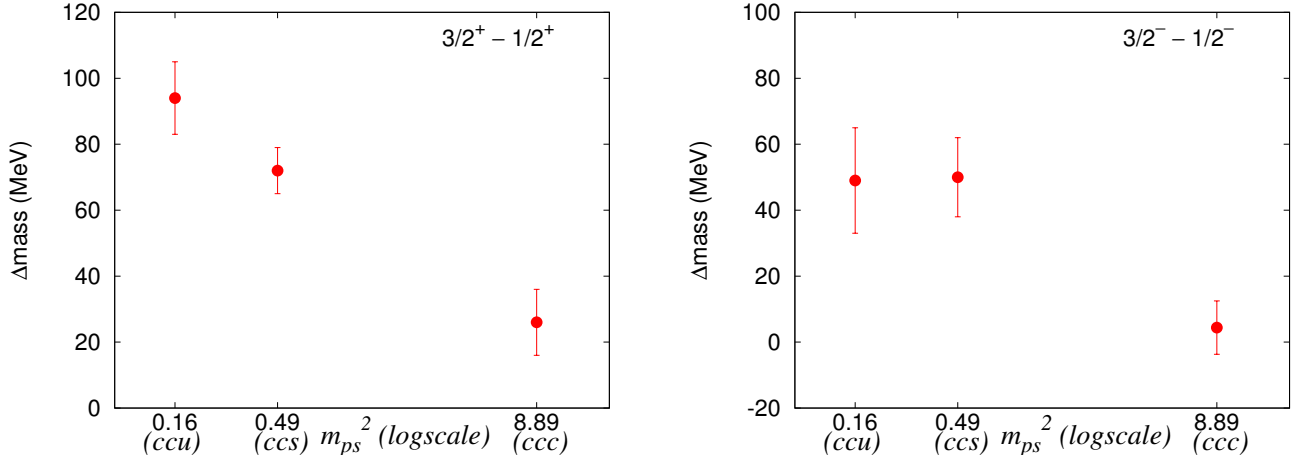


FIG. 16: Mass splittings between spin- $\frac{3}{2}^+$ and spin- $\frac{1}{2}^+$ states (left figure) and between spin- $\frac{3}{2}^-$ and spin- $\frac{1}{2}^-$ ground states (right figure) are compared for $\Xi_{cc}(ccu)$, $\Omega_{cc}(ccs)$ and $\Omega_{ccc}(ccc)$ baryons. For Ω_{ccc} , mass splitting is between $E_0(1/2^+)$ and $E_3(3/2^+)$ states, which is actually due to spin-orbit coupling, while for Ξ_{cc} and Ω_{cc} , these are between respective ground states and are due to hyperfine splittings.

The main results are shown in Figure 11 and Figure 12 for Ξ_{cc} and Ω_{cc} baryons, respectively. The ground states for spin 1/2 and 3/2, which have more relevance to recent experiments, are shown in Figure 9 and Figure 10. As in Ref. [42, 50], we also find bands of states with alternating parities and increasing energies. We also observed the number of extracted states of each spin in the three lowest-energy bands and the number of quantum numbers expected based on weakly broken $SU(6) \times O(3)$ symmetry agree perfectly, *i.e.*, the doubly-charmed baryon spectra remarkably resemble the expectations of quantum numbers from non-relativistic quark model [63–65]. This symmetry was also observed for light, strange [50] and triply-charmed baryon spectra [42]. For positive parity states this agreement does not get spoiled even with the inclusion of non-relativistic hybrid operators. However, it is expected that this band structure will persist with the inclusion of relativistic operators which contribute more to the higher excited states. The extracted spectra for the higher excited states also support this observation. Note our operator set does not include any multi-hadron operators. It is expected that inclusion of those operators, particularly those involving light

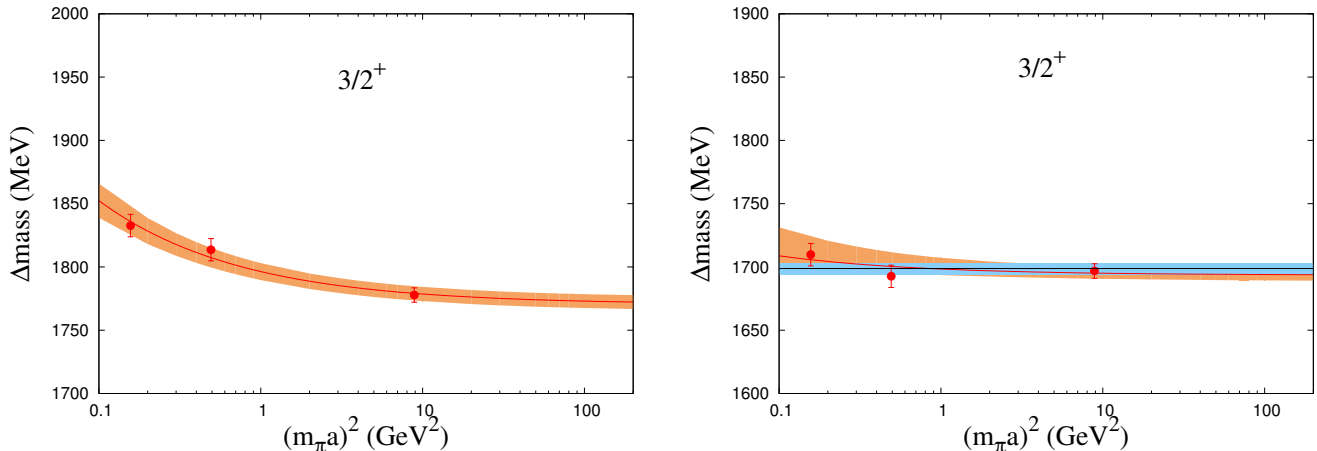


FIG. 17: Energy splittings between positive parity spin-3/2 baryons and pseudoscalar mesons as well as vector mesons are plotted against the square of the pseudoscalar masses. Left figure is the splittings of : $\Xi_{cc}^*(ccu) - D_u(\bar{c}u)$, $\Omega_{cc}^*(ccs) - D_s(\bar{c}s)$ and $\Omega_{ccc}^*(ccc) - \eta_c(\bar{c}c)$, and right figure includes following splittings : $\Xi_{cc}^*(ccu) - D_u^*(\bar{c}u)$, $\Omega_{cc}^*(ccs) - D_s^*(\bar{c}s)$ and $\Omega_{ccc}^*(ccc) - J/\psi(\bar{c}c)$; they are plotted against the square of the pseudoscalar masses (i.e., at D_u , D_s) and η_c mass. We fit the quark mass dependence with a form $a + b/m_{ps}$ (right figure is also fitted with a constant term). The fitted results are shown by solid lines with shaded regions as one sigma errorbars.

quarks, may modify some of these conclusions. We are also able to decode the structure of operators leading to a particular state: whether constructed by relativistic, non-relativistic, hybrids, non-hybrid types or a mixture of them all. However, this identification is not possible for negative parity states and highly excited positive parity states, as argued in Ref. [50].

Our calculated spectra do not support the chiral multiplet structure of doubly heavy baryons speculated in Refs. [14, 15]. The ground states of doubly charmed baryons are not degenerate and both for Ξ_{cc} and Ω_{cc} hyperfine splittings are around 80 – 100 MeV, as shown in fig 15. The calculated spectra do not match the diquark picture and instead they are remarkably similar to the expectations from non-relativistic quark models with an $SU(6) \times O(3)$ symmetry.

The study of the energy splittings between various excited states is quite helpful in revealing the nature of interquark interactions and a detailed knowledge of them could help to build successful models. We calculated hyperfine mass splittings between spin- $\frac{3}{2}^+$ and spin- $\frac{1}{2}^+$ states of Ξ_{cc} and Ω_{cc} and compared those with various other lattice and model predictions.

Energy splittings between the ground states of different spins were also evaluated and we observed that the hierarchy of the first few energy excitations in Ξ_{cc} and Ω_{cc} are quite similar. This indicates the involvement of similar dynamics to excite these states. To study the quark mass dependence of the energy splittings we compared results for $\Xi_{cc}(ccu)$, $\Omega_{cc}(ccs)$ and $\Omega_{ccc}(ccc)$ baryons for which there is a common ‘cc’ diquark and a varying quark from light to charm. Encouraged by a successful fitting of the mass splittings in triple-flavoured baryons [42] we studied similar mass splittings of doubly-charmed baryons. Here also we find that a heavy quark motivated form $a + b/m_{ps}$ can fit quite successfully energy splittings like : $\Xi_{cc}^*(ccu) - D_u(\bar{c}u)$, $\Omega_{cc}^*(ccs) - D_s(\bar{c}s)$ and $\Omega_{ccc}^*(ccc) - \eta_c(\bar{c}c)$, and $\Xi_{cc}^*(ccu) - D_u^*(\bar{c}u)$, $\Omega_{cc}^*(ccs) - D_s^*(\bar{c}s)$ and $\Omega_{ccc}^*(ccc) - J/\psi(\bar{c}c)$. From the fitted results we are able to predict $B_c^* - B_c = 80 \pm 8$ MeV and $\Omega_{ccb}^*(3/2^+) = 8050 \pm 10$ MeV.

V. ACKNOWLEDGEMENTS

We thank our colleagues within the Hadron Spectrum Collaboration. Chroma [43] and QUDA [44, 45] were used to perform this work on the Gaggle and Brood clusters of the Department of Theoretical Physics, Tata Institute of Fundamental Research, at Lonsdale cluster maintained by the Trinity Centre for High Performance Computing funded through grants from Science Foundation Ireland (SFI), at the SFI/HEA Irish Centre for High-End Computing (ICHEC), and at Jefferson Laboratory under the USQCD Initiative and the LQCD ARRA project. Gauge configurations were generated using resources awarded from the U.S. Department of Energy INCITE program at the Oak Ridge Leadership Computing Facility at Oak Ridge National Laboratory, the NSF Teragrid at the Texas Advanced Computer Center and the Pittsburgh Supercomputer Center, as well as at Jefferson Lab. MP acknowledges support from the Trinity College Dublin Indian Research Collaboration Initiative, Graduate school Tata Institute of Fundamental Research Mumbai and Austrian Science Fund (FWF):[I1313-N27]; NM acknowledges support from

Department of Theoretical Physics, TIFR; RGE acknowledges support from U.S. Department of Energy contract DE-AC05-06OR23177, under which Jefferson Science Associates, LLC, manages and operates Jefferson Laboratory;

-
- [1] The Review of Particle Physics : J. Beringer et al. (Particle Data Group), Phys. Rev. D **86**, 010001 (2012)
- [2] M. Mattson *et al.* [SELEX Collaboration], Phys. Rev. Lett. **89**, 112001 (2002) [hep-ex/0208014].
- [3] J. S. Russ [SELEX Collaboration], hep-ex/0209075.
- [4] A. Ocherashvili *et al.* [SELEX Collaboration], Phys. Lett. B **628**, 18 (2005) [hep-ex/0406033].
- [5] B. Aubert *et al.* [BABAR Collaboration], Phys. Rev. D **74**, 011103 (2006) [hep-ex/0605075].
- [6] R. Chistov *et al.* [BELLE Collaboration], Phys. Rev. Lett. **97**, 162001 (2006) [hep-ex/0606051].
- [7] Y. Kato *et al.* [Belle Collaboration], Phys. Rev. D **89**, no. 5, 052003 (2014) [arXiv:1312.1026 [hep-ex]].
- [8] R. Aaij *et al.* [LHCb Collaboration], JHEP **1312**, 090 (2013) [arXiv:1310.2538 [hep-ex]].
- [9] S. J. Brodsky, F. -K. Guo, C. Hanhart and U. -G. Meissner, Phys. Lett. B **698**, 251 (2011) [arXiv:1101.1983 [hep-ph]].
- [10] M. J. Savage and M. B. Wise, Phys. Lett. B **248**, 177 (1990).
- [11] M. J. Savage and R. P. Springer, Int. J. Mod. Phys. A **6**, 1701 (1991).
- [12] N. Brambilla, A. Vairo and T. Rosch, Phys. Rev. D **72**, 034021 (2005) [hep-ph/0506065].
- [13] S. Fleming and T. Mehen, Phys. Rev. D **73**, 034502 (2006) [hep-ph/0509313].
- [14] W. A. Bardeen, E. J. Eichten and C. T. Hill, Phys. Rev. D **68**, 054024 (2003) [hep-ph/0305049].
- [15] C. Quigg, arXiv:1109.5814 [hep-ph].
- [16] S. S. Gershtein, V. V. Kiselev, A. K. Likhoded, A. I. Onishchenko, Phys. Rev. D **62**, 054021 (2000).
- [17] V. V. Kiselev, A. K. Likhoded, O. N. Pakhomova and V. A. Saleev, Phys. Rev. D **66**, 034030 (2002) [hep-ph/0206140].
- [18] W. Roberts and M. Pervin, Int. J. Mod. Phys. A **23**, 2817 (2008) [arXiv:0711.2492 [nucl-th]].
- [19] D. Ebert, R. N. Faustov, V. O. Galkin and A. P. Martynenko, Phys. Rev. D **66**, 014008 (2002) [hep-ph/0201217].
- [20] A. P. Martynenko, Phys. Lett. B **663**, 317 (2008) [arXiv:0708.2033 [hep-ph]].
- [21] J. G. Korner, M. Kramer and D. Pirjol, Prog. Part. Nucl. Phys. **33**, 787 (1994) [hep-ph/9406359].
- [22] E. Bagan, M. Chabab and S. Narison, Phys. Lett. B **306**, 350 (1993).
- [23] V. V. Kiselev and A. K. Likhoded, Phys. Usp. **45**, 455 (2002) [Usp. Fiz. Nauk **172**, 497 (2002)] [hep-ph/0103169].
- [24] J. -R. Zhang and M. -Q. Huang, Phys. Rev. D **78**, 094007 (2008) [arXiv:0810.5396 [hep-ph]].
- [25] S. Narison and R. Albuquerque, Phys. Lett. B **694**, 217 (2010) [arXiv:1006.2091 [hep-ph]].
- [26] Z. -G. Wang, Eur. Phys. J. A **45**, 267 (2010) [arXiv:1001.4693 [hep-ph]].
- [27] R. Roncaglia, D. B. Lichtenberg and E. Predazzi, Phys. Rev. D **52**, 1722 (1995) [hep-ph/9502251].
- [28] L. Burakovsky, J. T. Goldman and L. P. Horwitz, Phys. Rev. D **56**, 7124 (1997) [hep-ph/9706464].
- [29] M. Rho, D. O. Riska and N. N. Scoccola, Phys. Lett. B **251**, 597 (1990).
- [30] N. Mathur, R. Lewis and R. M. Woloshyn, Phys. Rev. D **66**, 014502 (2002) [hep-ph/0203253].
- [31] R. Lewis, N. Mathur and R. M. Woloshyn, Phys. Rev. D **64**, 094509 (2001) [hep-ph/0107037].
- [32] J. M. Flynn *et al.* [UKQCD Collaboration], JHEP **0307**, 066 (2003) [hep-lat/0307025].
- [33] T. -W. Chiu and T. -H. Hsieh, Nucl. Phys. A **755**, 471 (2005) [hep-lat/0501021].
- [34] H. Na and S. A. Gottlieb, PoS LAT **2007**, 124 (2007) [arXiv:0710.1422 [hep-lat]].
- [35] L. Liu, H. -W. Lin, K. Orginos and A. Walker-Loud, Phys. Rev. D **81**, 094505 (2010) [arXiv:0909.3294 [hep-lat]].
- [36] H. -W. Lin, S. D. Cohen, L. Liu, N. Mathur, K. Orginos and A. Walker-Loud, Comput. Phys. Commun. **182** (2011) 24 [arXiv:1002.4710 [hep-lat]].
- [37] R. A. Briceño, H. -W. Lin and D. R. Bolton, Phys. Rev. D **86**, 094504 (2012) [arXiv:1207.3536 [hep-lat]].
- [38] C. Alexandrou, J. Carbonell, D. Christaras, V. Drach, M. Gravina and M. Papinutto, Phys. Rev. D **86**, 114501 (2012) [arXiv:1205.6856 [hep-lat]].
- [39] S. Basak, S. Datta, M. Padmanath, P. Majumdar and N. Mathur, PoS LATTICE **2012**, 141 (2012) [arXiv:1211.6277 [hep-lat]].
- [40] G. Bali, S. Collins and P. Perez-Rubio, J. Phys. Conf. Ser. **426**, 012017 (2013) [arXiv:1212.0565 [hep-lat]].
- [41] Y. Namekawa *et al.* [PACS-CS Collaboration], arXiv:1301.4743 [hep-lat].
- [42] M. Padmanath, R. G. Edwards, N. Mathur and M. Peardon, arXiv:1307.7022 [hep-lat].
- [43] J. J. Dudek, R. G. Edwards, N. Mathur and D. G. Richards, Phys. Rev. D **77**, 034501 (2008) [arXiv:0707.4162 [hep-lat]].
- [44] J. J. Dudek, R. G. Edwards, M. J. Peardon, D. G. Richards and C. E. Thomas, Phys. Rev. D **82**, 034508 (2010) [arXiv:1004.4930 [hep-ph]].
- [45] J. J. Dudek, R. G. Edwards, M. J. Peardon, D. G. Richards and C. E. Thomas, Phys. Rev. Lett. **103**, 262001 (2009) [arXiv:0909.0200 [hep-ph]].
- [46] J. J. Dudek, R. G. Edwards, M. J. Peardon, D. G. Richards and C. E. Thomas, Phys. Rev. D **83**, 071504 (2011) [arXiv:1011.6352 [hep-ph]].
- [47] L. Liu *et al.* [Hadron Spectrum Collaboration], JHEP **1207**, 126 (2012) [arXiv:1204.5425 [hep-ph]].
- [48] G. Moir, M. Peardon, S. M. Ryan, C. E. Thomas and L. Liu, arXiv:1301.7670 [hep-ph].
- [49] R. G. Edwards, J. J. Dudek, D. G. Richards and S. J. Wallace, Phys. Rev. D **84**, 074508 (2011) [arXiv:1104.5152 [hep-ph]].
- [50] R. G. Edwards, N. Mathur, D. G. Richards and S. J. Wallace, arXiv:1212.5236 [hep-ph].
- [51] J. J. Dudek and R. G. Edwards, Phys. Rev. D **85**, 054016 (2012) [arXiv:1201.2349 [hep-ph]].

- [52] R. G. Edwards, B. Joo and H. -W. Lin, Phys. Rev. D **78**, 054501 (2008) [arXiv:0803.3960 [hep-lat]].
- [53] H. -W. Lin *et al.* [Hadron Spectrum Collaboration], Phys. Rev. D **79**, 034502 (2009) [arXiv:0810.3588 [hep-lat]].
- [54] M. Peardon *et al.* [Hadron Spectrum Collaboration], Phys. Rev. D **80**, 054506 (2009) [arXiv:0905.2160 [hep-lat]].
- [55] E. E. Jenkins, Phys. Rev. D **54**, 4515 (1996) [hep-ph/9603449].
- [56] E. J. Eichten and C. Quigg, Phys. Rev. D **49**, 5845 (1994) [hep-ph/9402210].
- [57] E. B. Gregory, C. T. H. Davies, E. Follana, E. Gamiz, I. D. Kendall, G. P. Lepage, H. Na and J. Shigemitsu *et al.*, Phys. Rev. Lett. **104**, 022001 (2010) [arXiv:0909.4462 [hep-lat]].
- [58] E. B. Gregory, C. T. H. Davies, I. D. Kendall, J. Koponen, K. Wong, E. Follana, E. Gamiz and G. P. Lepage *et al.*, Phys. Rev. D **83**, 014506 (2011) [arXiv:1010.3848 [hep-lat]].
- [59] C. McNeile, C. T. H. Davies, E. Follana, K. Hornbostel and G. P. Lepage, Phys. Rev. D **86**, 074503 (2012) [arXiv:1207.0994 [hep-lat]].
- [60] P. Hasenfratz, R. R. Horgan, J. Kuti and J. M. Richard, Phys. Lett. B **94**, 401 (1980).
- [61] B. Silvestre-Brac, Few Body Syst. **20**, 1 (1996).
- [62] Z. S. Brown, W. Detmold, S. Meinel and K. Orginos, Phys. Rev. D **90**, no. 9, 094507 (2014) [arXiv:1409.0497 [hep-lat]].
- [63] O. W. Greenberg, Phys. Rev. Lett. **13**, 598 (1964).
- [64] N. Isgur and G. Karl, Phys. Lett. B **72**, 109 (1977).
- [65] N. Isgur and G. Karl, Phys. Rev. D **18**, 4187 (1978).
- [66] R. G. Edwards *et al.* [SciDAC and LHPC and UKQCD Collaborations], Nucl. Phys. Proc. Suppl. **140**, 832 (2005) [hep-lat/0409003].
- [67] M. A. Clark, R. Babich, K. Barros, R. C. Brower and C. Rebbi, Comput. Phys. Commun. **181**, 1517 (2010) [arXiv:0911.3191 [hep-lat]].
- [68] R. Babich, M. A. Clark and B. Joo, arXiv:1011.0024 [hep-lat].